

Theoretical and Electrochemical Study of Carbon Steel Corrosion Inhibition in the Presence of Two Synthesized Schiff Base Inhibitors: Application of Fast Fourier Transform Continuous Cyclic Voltammetry to Study the Adsorption Behavior

Shirin Shahabi¹, Parviz Norouzi^{1,2,*}, Mohammad Reza Ganjali²

¹ Center of Excellence in Electrochemistry, Faculty of Chemistry, University of Tehran, Tehran, Iran

² Biosensor Research Center, Endocrinology & Metabolism Molecular-Cellular Sciences Institute, Tehran University of Medical Sciences, Tehran, Iran

*E-mail: norouzi@khayam.ut.ac.ir

Received: 19 November 2014 / Accepted: 25 December 2014 / Published: 19 January 2015

The inhibition effect of two new synthesized Schiff bases, (E)-2-hydroxy-N'-(pyridin-2-ylmethylene) benzohydrazide (S₁) and (E)-2-hydroxy-N'-(thiophen-2-ylmethylene) benzohydrazide (S₂), on the carbon steel corrosion in 1.0 M HCl was investigated by Potentiodynamic Polarization, Electrochemical Impedance Spectroscopy, Scanning Electron Microscopy and Fast Fourier Transform Continuous Cyclic Voltammetry. The results showed that both Schiff bases were mixed-type corrosion inhibitors. They affected the corrosion rate by adsorption on the carbon steel surface. The inhibition efficiencies increased with increasing the inhibitors concentration in the corrosive solution. Differential continuous cyclic voltammograms showed that although S₂ was a more effective inhibitor than S₁, the adsorption of S₁ occurred more rapidly than S₂. Finally, the study was supplemented by performing the quantum chemical calculations at the level of DFT/B3LYP with 6-31G(d,p) basis set. The calculation results were in good agreement with the obtained experimental data.

Keywords: Corrosion inhibition; carbon steel; FFT Voltammetry; quantum chemical calculations

1. INTRODUCTION

Acid solutions such as HCl and H₂SO₄ are generally used in industrial acid descaling and pickling processes, oil well acidification and cleaning of boilers to remove surface contaminations like lime scale, rust, etc. from the metals [1-4]. HCl is the primary acid used in pickling processes.

The advantageous properties of carbon steel such as excellent mechanical properties and low cost make it the main metal used in industrial means [5]. Like most of frequently used metals, carbon steel needs to be cleaned before, during and after fabrication to eliminate or lessen the fouling from equipment and piping. In spite of removing the specific deposits from the steel surface through the acid cleaning process, the disadvantage is that the acid can also dissolve the actual metal surface and cause its corrosion. For this reason, it is important to decrease this undesirable reaction. The corrosion of steel can be greatly decreased using addition of inhibitors to the acid solution [6, 7]. Inhibitors are chemicals, which are added to the corrosive medium with the objective of adsorbing on the metal surface and reducing the corrosion rate. Most of organic compounds that are usually used as corrosion inhibitors have heteroatoms and electron reached groups in their molecular structures. Generally, organic inhibitors modify the entire surface of the corroding metal. So, both anodic and cathodic effects would be expected in the presence of organic inhibitors. Schiff bases are organic compounds that can be simply synthesized from low-cost materials. They could be applied as corrosion inhibitors for steel [8-10], copper [11, 12] and aluminum [13, 14].

In recent years, the developments in both software and hardware cause the use of computational methods to extend in various fields [15-19]. Among them is the utilization of quantum chemical calculations (QCCs) in the corrosion inhibition studies [20-27]. By performing these calculations, it could be possible to characterize the molecular structure of organic inhibitors by calculated electronic and geometrical parameters and analyze the inhibition mechanism and interactions between the inhibitors and metallic surface.

In our attempt to find suitable and efficient inhibitors, we introduced in this paper, two synthesized Schiff bases (E)-2-hydroxy-N'-(pyridin-2-ylmethylene)benzohydrazide (S_1) and (E)-2-hydroxy-N'-(thiophen-2-ylmethylene) benzohydrazide (S_2) as new efficient carbon steel corrosion inhibitors in 1.0 M HCl. Their inhibition effect was evaluated by Tafel polarization and Electrochemical Impedance Spectroscopy (EIS). Moreover, the Scanning Electron Microscopy (SEM) was used to study the surface morphology of carbon steel in 1.0 M HCl solution with and without the inhibitors S_1 and S_2 . Fast Fourier Transform Continuous Cyclic Voltammetry (FFTCCV) was utilized to study the adsorption behavior of S_1 and S_2 on the steel surface. Using FFTCCV, it was possible to continuously monitor the changes in current and charge passed through the electrode during its immersion in the corrosive solution, which was not practicable by other electrochemical techniques such as PDP and EIS, which are routinely used in this research field. Finally, QCC was done to investigate the effect of the inhibitors molecular structure on the inhibition efficiencies and find information about the inhibition mechanism.

2. EXPERIMENTAL

2.1. Synthesize of Schiff bases

Figure 1 shows the molecular structures of Schiff bases, S_1 and S_2 , which was used as carbon steel corrosion inhibitors in this paper. In order to synthesize S_1 , A mixture of 2-

hydroxybenzohydrazine (0.01 moles), pyridine-2-carbaldehyde (0.01 moles) and a catalytic amount of PTSA was refluxed in ethanol (100 mL) for 4 h. Then the solvent was evaporated to 40 mL. To synthesize S_2 , A mixture of 2-hydroxybenzohydrazine (0.01 moles), thiophene-2-carbaldehyde (0.01 moles) and a catalytic amount of acetic acid was refluxed in ethanol (70 mL) for 2 h. Then the solvent was evaporated to 20 mL. After cooling to room temperature, the products, S_1 and S_2 , were obtained as crystals.

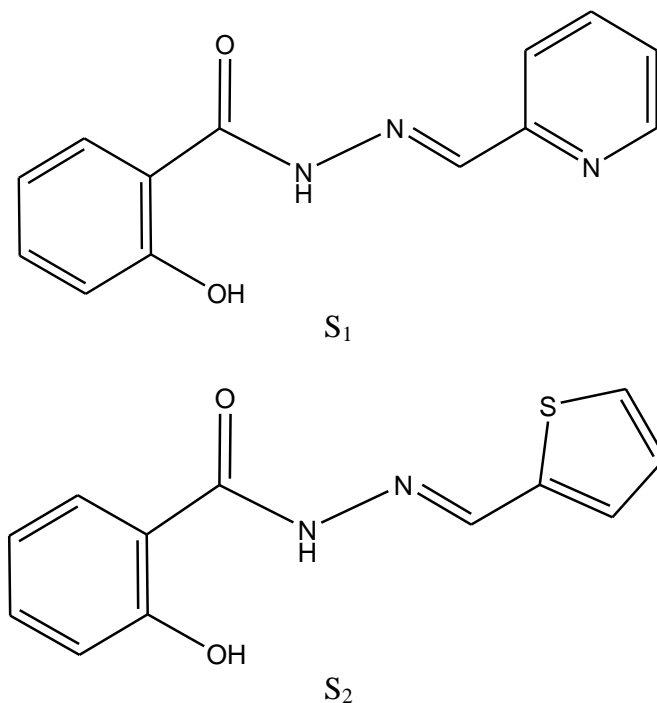


Figure 1. Molecular structures of inhibitors S_1 and S_2 .

2.2. Carbon steel samples

The specimens containing C 0.326 %, Si 0.235 %, Mn 0.742 %, P 0.016 %, Cr 0.073 %, Ni 0.015 %, Al 0.022 %, S 0.017 %, Cu 0.129 %, V 0.002 % and the rest iron was used as the working electrode for all experiments. Before doing each measurement, the electrode surface was polished with different grades of emery papers (which ended with the 1200 grit), degreased in ultrasonic bath with ethanol and acetone and finally rinsed with distilled water.

2.3. Solutions

The aggressive solution of analytical grade of 1.0 M HCl was prepared by dilution of 36 % HCl from Merck with distilled water. The inhibitor solutions were prepared in 1.0 M HCl containing 5 % v/v DMSO because of the solubility problems. Obviously, this volume of DMSO was also added to the blank solution.

2.4. Polarization measurements

Polarization studies were performed using an AUTOLAB model PGSTAT30 and a three-electrode set-up containing a Pt counter electrode (CE), an Ag/AgCl reference electrode (RE) and a carbon steel working electrode (WE). The WE was constructed from a cylindrical carbon steel bar mounted in epoxy resin to give an exposed surface of 5 mm diameter. prior to obtaining polarization curves, the fresh surface of WE was immersed in the test solution for 45 minutes to reach a steady state open circuit potential (E_{ocp}). After reaching E_{ocp} , the potential was swept from a more positive potential than E_{ocp} to a more negative potential than E_{ocp} at a scan rate of 1 mV/s. The potentiodynamic polarization curves were recorded using a personal computer, which was connected to the electrochemical instrument. The polarization data was analyzed using GPES electrochemical software. The inhibition efficiency (IE %) was defined according the Eq. (1) [31]:

$$IE \% = \frac{I_{corr,uninhibit} - I_{corr,inhibit}}{I_{corr,uninhibit}} \times 100 \quad (1)$$

where the $I_{corr,uninhibit}$ and $I_{corr,inhibit}$ are the corrosion current density without and with inhibitors, respectively.

2.5. EIS measurements

The electrochemical impedance measurements were performed using the same instrument and cell set-up used for the polarization measurements. The EIS experiments were carried out at E_{ocp} by superimposing a sinusoidal potential of 5mV amplitude at frequencies between 5×10^{-2} - 10^5 Hz. EIS data were analyzed with FRA software. Polarization resistance (R_p) and constant phase element (CPE) were obtained from Nyquist plots. R_p is inversely proportional to corrosion current density. So, it is used to calculate the IE% using the Eq. (2) [32]:

$$IE \% = \frac{R_{p,inhibit} - R_{p,uninhibit}}{R_{p,inhibit}} \times 100 \quad (2)$$

where $R_{p,inhibit}$ and $R_{p,uninhibit}$ are the polarization resistance of inhibited and uninhibited solutions, respectively.

2.6. SEM measurements

The surface morphology of carbon steel samples was observed using a Hitachi-460 SEM after immersing the samples in 1.0 M HCl solution for 24 h with and without inhibitors. The employed acceleration beam energy was 20.0 kV.

2.7. FFTCCV experiments

To perform FFTCCV experiments, a set-up containing a PC equipped with a data acquisition board (PCL-818HG, Advantech. Co.) and a custom-made potentiostat was used with a three-electrode configuration that was the same as polarization and EIS electrodes. At each FFTCCV run, repeatedly

cyclic voltammograms were obtained by sweeping the potential between an initial and a final potential. This range contained corrosion potential (E_{corr}). Although the effect of corrosion inhibitors were usually studied at low potential scan rates, due to the instrument limitations, the CV measurements were carried out at 1.0 V/s, which was the lowest possible scan rate that could be used.

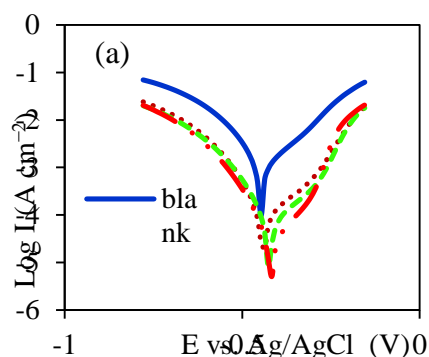
2.8. Quantum chemical calculations

The geometrically optimization of molecular structures of the studied Schiff bases were done by Gaussian03 [33] software using the density functional theory (DFT) at the B3LYP/6-31G(d,p) level of theory. The calculated quantum chemical parameters are the highest occupied molecular orbital energy (E_{HOMO}), the lowest unoccupied molecular orbital energy (E_{LUMO}), the energy gap between HOMO and LUMO (ΔE) and the dipole moment (D).

3. RESULTS AND DISCUSSION

3.1. Polarization curves

Figure 2a and b represent typical polarization curves for carbon steel electrode in 1.0 M HCl in the absence and presence of different concentrations of the Schiff bases S_1 and S_2 , respectively. This figure shows that with addition of the inhibitors, the Tafel curve shifts to lower current densities and this shift is more pronounced for the anodic branch. By performing Tafel extrapolation analysis to these curves, the electrochemical parameters of the corrosion process, such as corrosion potential (E_{corr}), corrosion current density (I_{corr}), cathodic and anodic Tafel slopes (b_a and b_c) are calculated and shown in Table 1. The Table demonstrates that the addition of inhibitors makes changes to both anodic and cathodic Tafel slopes suggesting these Schiff bases hinder either anodic dissolution of iron or cathodic evolution of H_2 . These results could be due to the adsorption of the inhibitors on the surface of carbon steel, which causes blocking the active sites of surface.



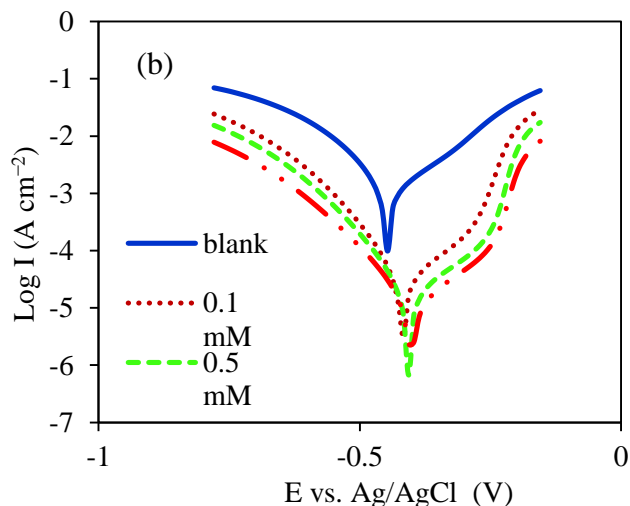


Figure 2. Polarization curves of carbon steel in 1.0 M HCl solution without and with different concentrations of (a) inhibitor S_1 and (b) inhibitor S_2 .

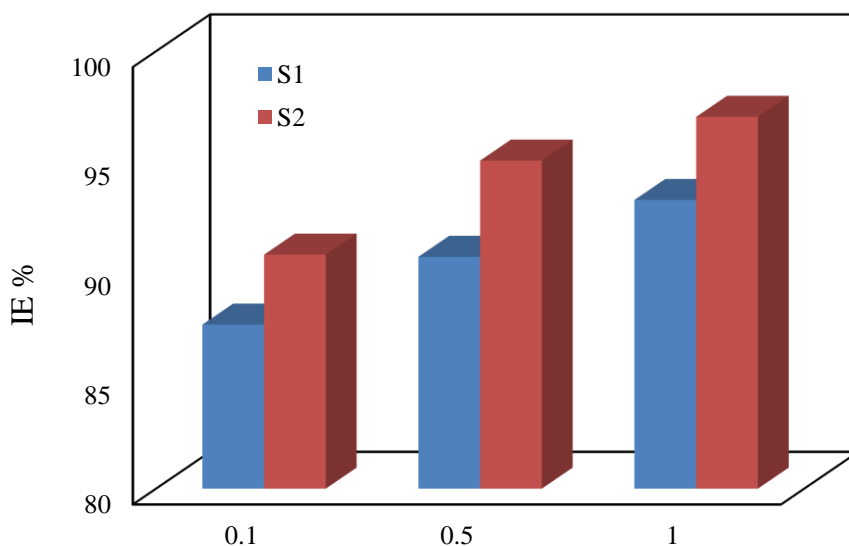


Figure 3. Plot of IE % values, obtained by polarization method, vs. S_1 and S_2 concentration.

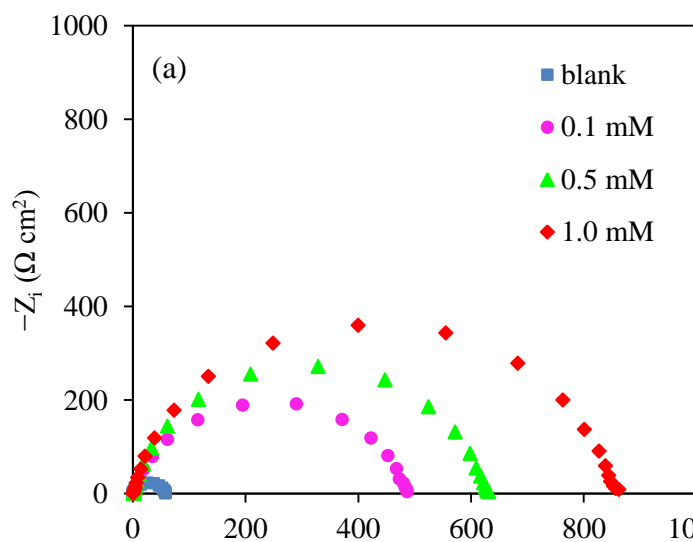
Furthermore, it is clear that the addition of S_1 and S_2 to 1.0 M HCl causes I_{corr} to decrease to lower values and this reduction are more noticeable with increasing the inhibitors concentration. The IE % values, obtained based on I_{corr} , for S_1 and S_2 versus the inhibitor concentration, were plotted In Figure 3. The results of polarization method show that the maximum values of IE % were obtained for 1.0×10^{-3} M of S_2 that equals 97.0 %. Moreover, the maximum shift in E_{corr} (53 mV toward anodic potentials) was also seen for 1.0×10^{-3} M of S_2 , proposing the mixed-type action of the investigated Schiff bases with predominantly anodic inhibition [34, 35]. The obtained results indicate that S_2 is a more effective corrosion inhibitor than S_1 .

Table 1. Polarization parameters for carbon steel in 1.0 M HCl solution in the absence and presence of various concentrations of the inhibitors S₁ and S₂.

Inhibitor	C _{inh} (M)	-E _{corr} (mV)	I _{corr} (μA cm ⁻²)	-b _c (mV dec ⁻¹)	b _a (mV dec ⁻¹)	IE (%)
Blank	-	455	461.3	137	111	-
S ₁	1.0×10 ⁻⁴	420	57.4	135	119	87.5
	5.0×10 ⁻⁴	439	43.5	139	124	90.6
	1.0×10 ⁻³	419	31.4	141	124	93.2
S ₂	1.0×10 ⁻⁴	441	43.3	144	127	90.7
	5.0×10 ⁻⁴	439	23.1	151	129	95.0
	1.0×10 ⁻³	402	14.1	156	122	97.0

3.2. Electrochemical Impedance Spectroscopy

Figure 4a and b demonstrate the impedance spectra (Nyquist plots) for carbon steel in 1.0 M HCl in the absence and presence of the Schiff bases. As can be seen, addition of the inhibitors leads to expansion of the semicircles diameter and the extent of this enlargement is proportional with the inhibitors concentrations. For these curves, the simplest circuit for describing the metal/solution interface is -R(CR)- which is shown in Figure 5. Such equivalent circuit has been previously used to model the metal/acid interface [7, 9]. In the circuit, CPE is the constant phase element, R_s and R_p are successively the solution and the polarization resistances, and n is the phase shift (-1 ≤ n ≤ 1) that represents degree of surface inhomogeneity [36, 37]. CPE is used instead of double layer capacitance to describe deviations induced by surface roughness and dispersion effects. For n= 0, 1 and -1, the CPE denotes a pure resistor, capacitor or inductor, respectively.



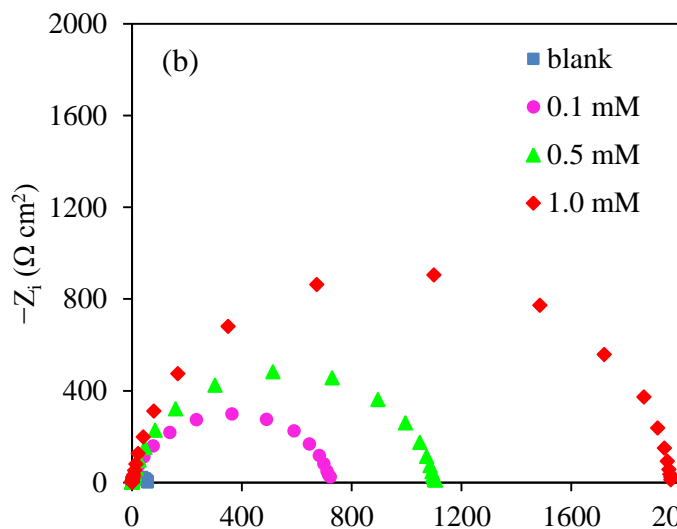


Figure 4. Nyquist Impedance plots of carbon steel obtained in 1.0 M HCl in the presence of various concentrations of (a) S₁ and (b) S₂.

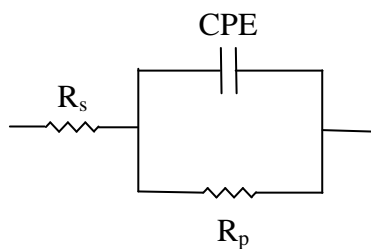


Figure 5. Equivalent circuit of the impedance spectra.

Table 2. Electrochemical impedance parameters for carbon steel in 1.0 M HCl solution in the absence and presence of various concentrations of the inhibitors S₁ and S₂.

Inhibitor	C _{inh} (M)	R _p (Ω cm ²)	n	Q (μΩ ⁻¹ s ⁿ cm ⁻²)	IE (%)
Blank	–	57.8	0.86	305.7	–
S1	1.0×10 ⁻⁴	486.4	0.86	36.4	88.1
	5.0×10 ⁻⁴	622.9	0.92	27.3	90.7
	1.0×10 ⁻³	850.1	0.90	25.6	93.2
S2	1.0×10 ⁻⁴	735.5	0.87	31.5	92.1
	5.0×10 ⁻⁴	1100.1	0.92	18.3	94.7
	1.0×10 ⁻³	1950.3	0.96	11.2	97.0

The results show that for our system $0 < n < 1$, therefore, the double layer is not an ideal capacitor. The impedance function of a CPE takes the form [38]:

$$Z_{\text{CPE}} = Q^{-1} (j\omega)^{-n} \quad (3)$$

where Q is the magnitude of CPE, j displays the imaginary number, ω is the sine wave angular frequency ($\omega = 2\pi f$, the frequency in Hz) and n is the phase shift.

The calculated impedance parameters, namely the values of R_p , n , Q and IE % are shown in Table 2. The values of IE % were calculated using Eq. 2. In this table, it can be noticed that for both inhibitors, the R_p values grow proportionally with the inhibitors concentration, which could be due to more adsorption of the Schiff bases on the electrode surface. Based on the results, the decrease in Q values could be due to replacement of adsorbed water molecules and ions by the larger organic molecules. This replacement extends the double layer distance and so, reduces its capacitance. Again, the values of IE % for S_2 are greater than S_1 , which confirms Tafel polarization results.

3.3. Surface analysis

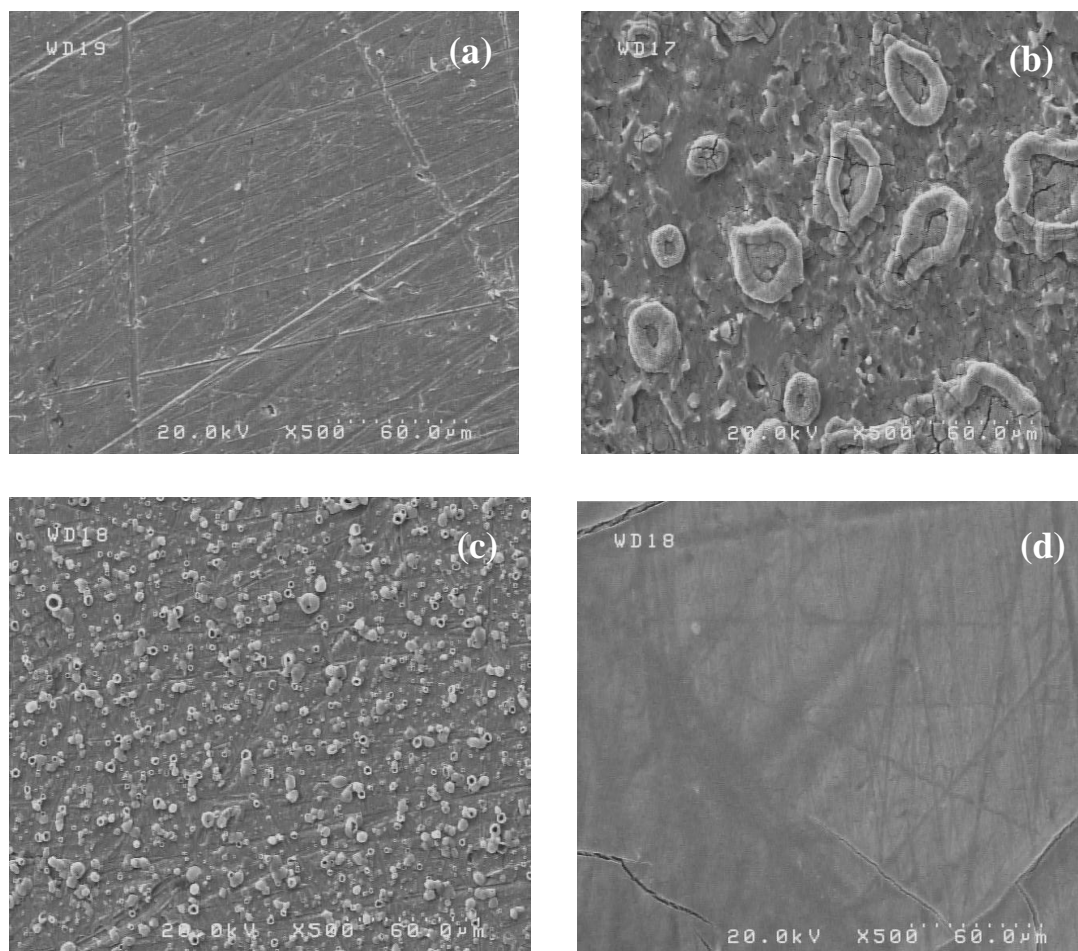


Figure 6. SEM micrographs of carbon steel for freshly polished surface (a), after 24 h immersion in 1.0 M HCl without inhibitors (b) and with 1.0×10^{-3} M of S_1 (c) and S_2 (d).

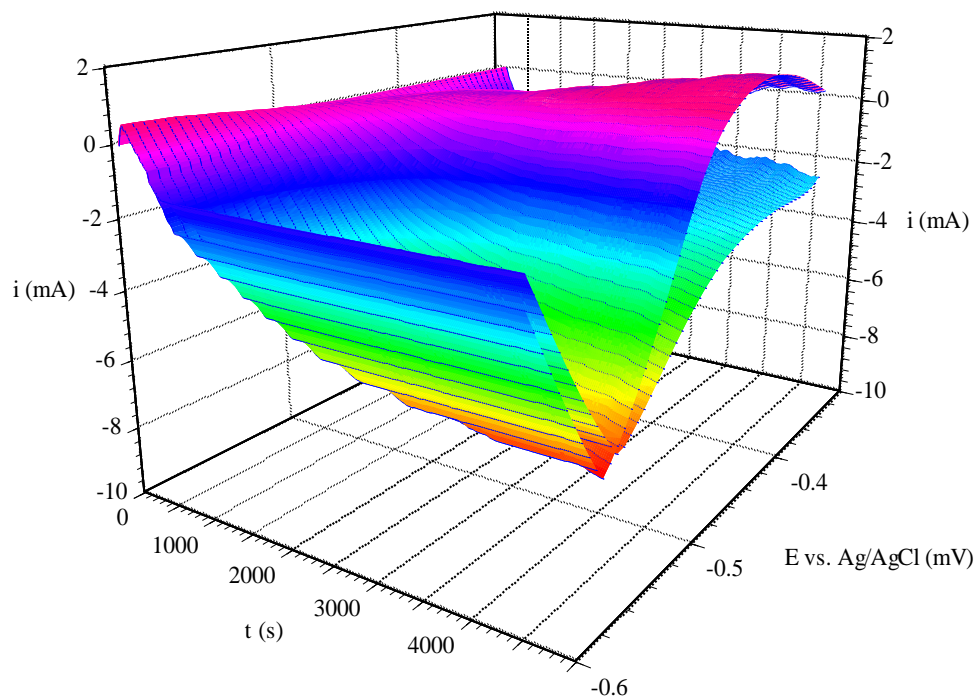
Figure 6 illustrates the SEM images of (a) fresh carbon steel surface, (b) after 24 h immersion in 1.0 M HCl without inhibitors and (c) with 1.0×10^{-3} M S_1 and (d) S_2 . Figure 6b represents highly corroded surface with a large number of deep cavities and cracks due to immersion in acid. However, when we add the S_1 to the acidic solution, as shown in Figure 6c, the size of the cavities noticeably decreases. Moreover, as shown in Figure 6d, the maximum surface protection was seen for the solution containing inhibitor S_2 , in which most of corrosion cavities and cracks are removed from the steel surface. These results confirm that S_2 inhibits the carbon steel corrosion more effectively than S_1 , which is in agreement with above electrochemical results.

3.4. FFTCCV measurements

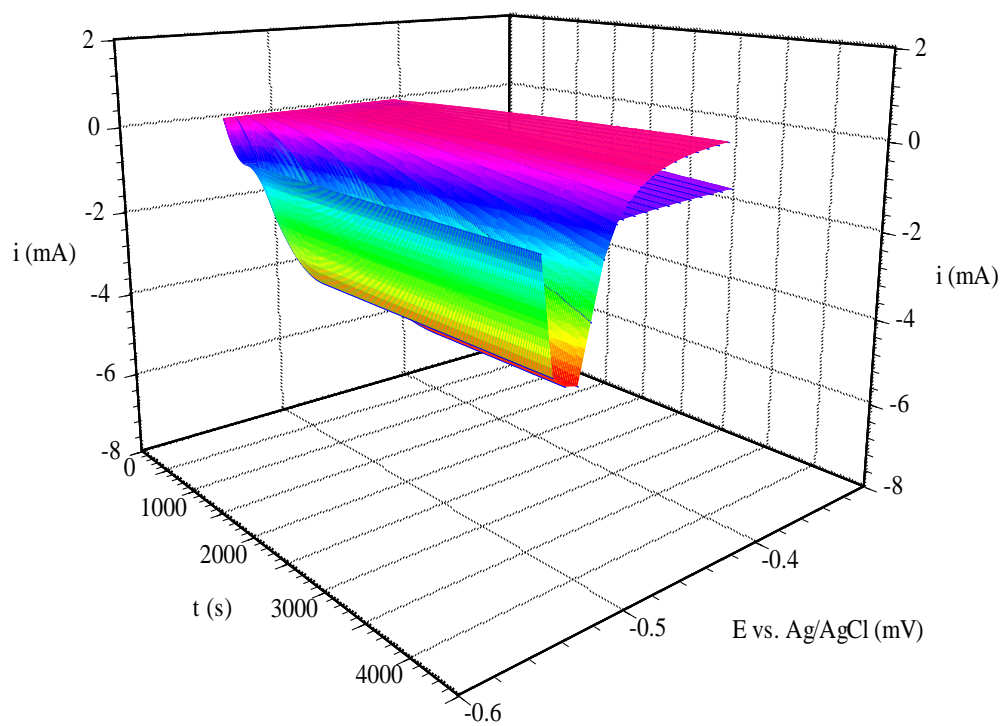
In order to follow the adsorption behavior of two inhibitors on the electrode surface, FFTCCV was used. In this technique, the cyclic potential waveform was applied continuously on the electrode surface. At the end of each experiment, we would have numerous cyclic voltammograms, which are recorded continuously at real time. These continuous recorded CV curves contain information about the metal surface changes during immersion time. To calculate the response of the electrode, at the first of each experiment, the background current was subtracted from the first CV curve. The value of current change over a potential range, E_1 and E_2 , was calculated by following equation [39-41]:

$$\Delta i(s, E) = i(s, E) - i(s_r, E) \quad (4)$$

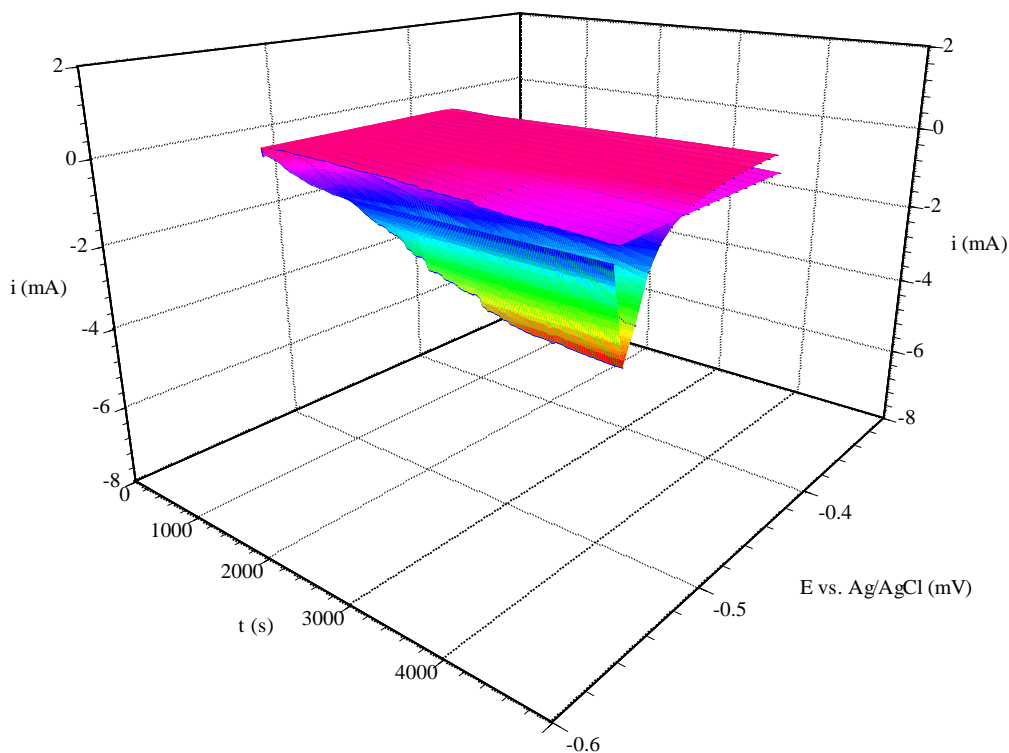
where s is the sweep number, $i(s, E)$ represents the CV curve recorded during the s -th sweep and $i(s_r, E)$ is the reference CV curve. By continuously applying the potential waveform and performing the subtraction shown in Eq. 4, it was possible to nonstop monitor the changes in current and charge passed through the electrode. Figure 7 shows the typical subtracted 3-D CVs for carbon steel samples in different solutions. In this figure, all CVs were subtracted from the reference CV. Figure 7a represents the differential CVs of the working electrode in the 1.0 M HCl solution during 70 minutes without any inhibitors. As can be seen, the net current change with the time is significantly large (up to 8.0 mA) during 70 minutes and the current change is progressively enhanced by applying subsequent CVs. Figure 7b shows the differential CVs for the steel electrode in the solution containing 5.0×10^{-4} M of S_1 . The graph demonstrates that the slope of net current change is smaller than the previous experiment (Figure 7a). This is an indication of inhibition of the corrosion by S_1 molecules, which are adsorbed on the steel surface. The figure also shows that the current variation reaches a plateau (3.6 mA) after 1500 s, which is an indication of the maximum surface coverage by S_1 . Figure 7c represents the subtracted 3-D CVs of the electrode in the solution including 5.0×10^{-4} M S_2 . In this experiment, the net current change increased up to 3000 s, and after that, remained constant (2.8 mA). The obtained results from the FFTCCV indicate that S_1 molecules adsorb faster than S_2 on the electrode surface, therefore, in shorter time the corrosion current reaches to a near constant value. In other words, S_2 molecules need more time to reach their maximum surface coverage, but the quantity of maximum coverage for S_2 molecules are better than S_1 molecules.



(a)



(b)



(c)

Figure 7. Differential cyclic voltammograms of carbon steel electrode recorded during 70 minutes immersion in 1.0 M HCl solution without (a) and with 5.0×10^{-4} M S_1 (b) and S_2 (c).

FFTCCV method gives information about the adsorption process by calculating the amount of charge (ΔQ) that passes through the electrode during applying potential waveform. The value of ΔQ is calculated by integrating the current changes between potentials E_1 to E_2 , which is the potential range of corrosion process.

$$Q_t = \frac{1}{v} \int_{E_1}^{E_2} I(E) dE \tag{5}$$

where v is the scan rate. In reality, voltammograms are recorded numerically by sampling current in equal time intervals. Therefore, CV curves are recorded numerically, and the current integration over a potential range, E_1 and E_2 , was calculated by this numerical equation [42-44]:

$$\Delta Q(s,t) = \Delta t \left(\sum_{E=E_1}^{E=E_2} I(s,E) - \sum_{E=E_1}^{E=E_2} I(s_r,E) \right) \tag{6}$$

where s is the sweep number, t is the time period between subsequent sweeps, Δt is the time difference between two subsequent points on the CV curves, $i(s, E)$ represents the CV curve recorded during the s -th sweep and $i(s_r, E)$ is the reference CV curve. The reference CV curve was obtained by averaging three CVs recorded at the beginning of the experiment.

Figure 8 represents the plot of ΔQ as a function of time for carbon steel electrode in the absence and presence of 5.0×10^{-4} M of S_1 and S_2 after 70 minutes. The change of ΔQ in time shows that in the absence of inhibitors, the corrosion is in its maximum rate. Addition of the inhibitors reduces the slope of ΔQ - t plot, which is an indication of reducing the corrosion rate. As can be seen in the figure, this effect for the addition of S_2 is greater than S_1 . Consequently, it can be concluded that

the S_2 inhibits the carbon steel corrosion more effectively than S_1 , which is in agreement with potentiodynamic polarization, EIS and SEM results. Like that previously seen for the maximum current change in differential continuous cyclic voltammograms, the ΔQ reaches to an almost constant level, too. For the solution containing S_1 , after about 1500 s, the ΔQ change becomes much slower and its value remains almost unchanged. This time is 3000 s for the solution containing S_2 . In contrast, the level of constant value for carbon steel electrode in the presence of S_1 is clearly greater than S_2 . This observation indicates that inhibitor S_2 adsorbs more slowly than S_1 , but its adsorption is more robust and operative. Therefore, S_2 is a more effective corrosion inhibitor for carbon steel corrosion in HCl solution.

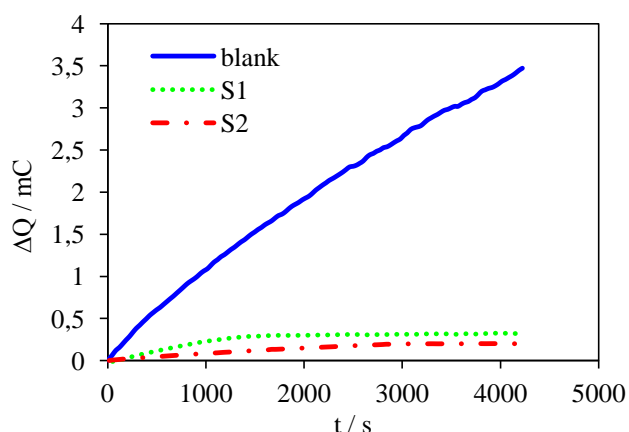


Figure 8. Plot of total charge loaded by the carbon steel electrode (ΔQ) vs. time in the blank solution and the solution containing 5.0×10^{-4} M of S_1 and S_2 .

3.5. Quantum chemical parameters

Figure 9a, b and c respectively show the optimized geometry, the HOMO density distribution and the LUMO density distribution for S_1 and S_2 molecules. The optimized geometry, the HOMO and the LUMO density distribution of S_2 are represented successively in Figure 9d, e and f. As previously mentioned, the calculations were done by Gaussian03 with DFT method and B3LYP level of theory using 6-31G(d,p) basis set. The structures are sketched with GaussView5 software [45].

Calculation of HOMO and LUMO energies and their density distribution study were done to get information about the global reactivity of molecules. The optimized geometries of S_1 and S_2 have planar structure that is favorable for effectively adsorption of inhibitor molecules with maximum contact area between the adsorbed molecules and the metal surface.

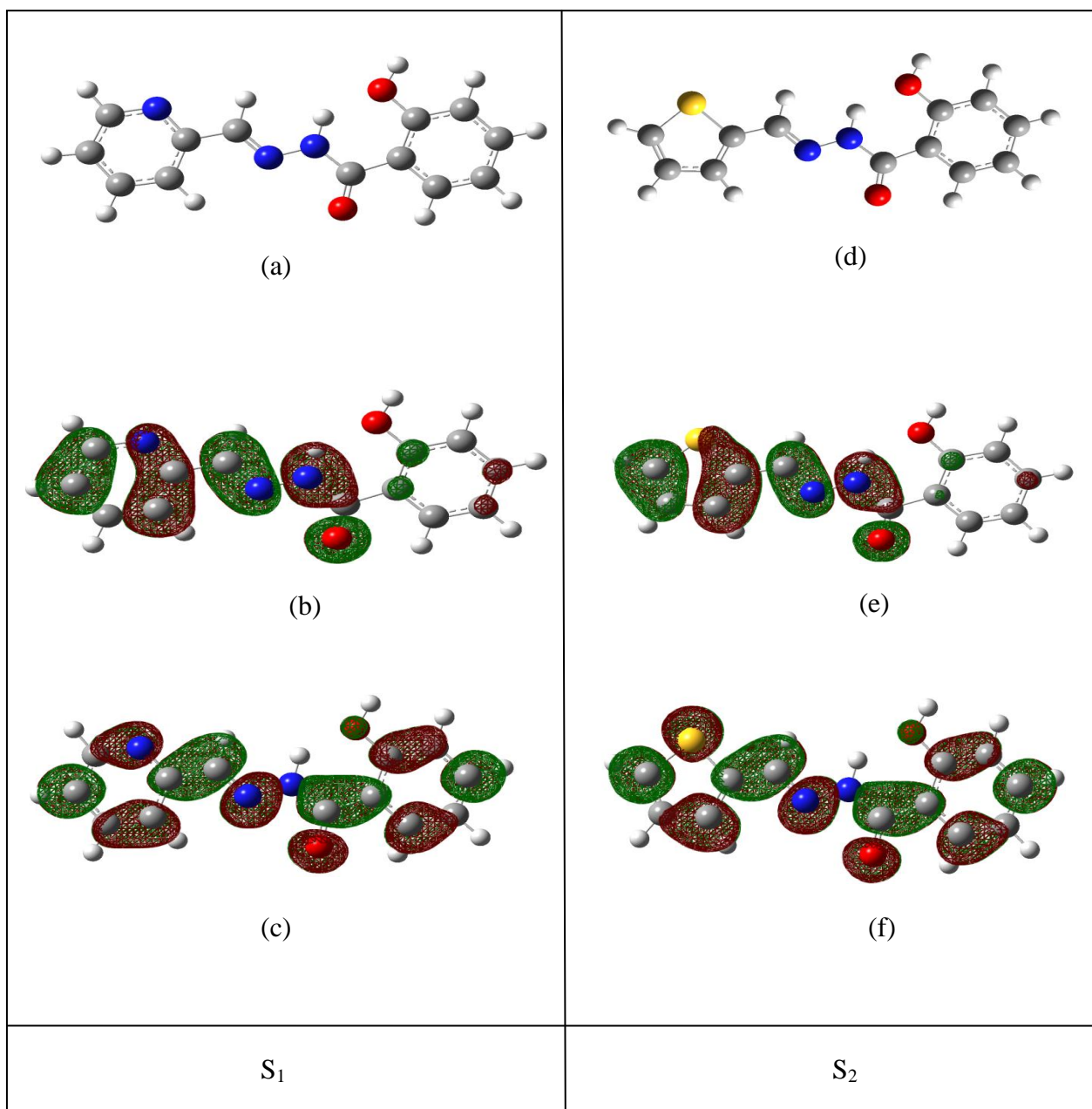


Figure 9. Optimized geometries of studied Schiff bases S_1 (a) and S_2 (d), density distribution of HOMO for S_1 (b) and S_2 (e) and density distribution of LUMO for S_1 (c) and S_2 (f).

Table 3 represents the quantum chemical parameters calculated for the studied Schiff base molecules. E_{HOMO} measures the electron donating ability of a compound to an appropriate acceptor molecule with low-energy empty molecular orbital. An inhibitor with higher HOMO energy can easily provide electrons for metallic substrate to adsorb on its surface [47-49]. On the other hand, E_{LUMO} reveals the tendency of a molecule to receive electrons. A molecule with lower LUMO energy would be a better electron acceptor from a donor molecule [46-49]. It has been reported that the inhibitor molecules can be adsorbed not only by donating electrons from their HOMO orbitals of Fe, but also by receiving electrons from 3d-orbitals of Fe to their LUMO molecular orbitals leading to create a feedback bond [47-49]. Figure 9, also, shows that S_1 and S_2 are similar in HOMO and LUMO distributions.

The HOMO for both molecules has the minimum density on the phenolic group, which is bound to carbonyl group and the LUMO is nearly distributed on the whole molecule.

Table 3. Some quantum chemical parameters for the studied Schiff bases calculated using B3LYP/6-31G(d,p).

Inhibitor	E_{HOMO} (eV)	E_{LUMO} (eV)	ΔE (eV)	D (Debye)
S ₁	-5.99	-1.60	4.39	4.12
S ₂	-5.57	-1.53	4.04	5.28

As listed in Table 3, The HOMO energy value is -5.99 eV for S₁ and -5.57 eV for S₂, illustrating that S₂ can donate electrons more easily than S₁ and it acts as a better corrosion inhibitor. Another parameter computed by QCCs is the energy gap between HOMO and LUMO ($\Delta E = E_{\text{LUMO}} - E_{\text{HOMO}}$), which represents a measure of reactivity of the molecule. By decreasing ΔE , polarizability of the molecule increases and the softness properties become more pronounced. The smaller value of ΔE can lead to more effective adsorption and higher inhibition efficiency [47, 48]. ΔE values showed in Table 3 are in good agreement with the experimental results. Values of LUMO energies of S₁ (-1.60 eV) and S₂ (-1.53 eV) cannot explain the inhibition effects based on the concept of relationship between E_{LUMO} values and the ability of molecule toward accept electrons from a donor molecule. However, the presence of sulphur atom in the thiophene ring of the Schiff base S₂ results in overlapping of 3d-electrons from Fe orbitals with 3d-vacant orbitals of sulphur and formation of $d\pi-d\pi$ bond. This phenomenon enhances the inhibition effect of S₂ rather than S₁, which has pyridine ring instead of thiophene ring [3, 48-50]. Dipole moment (D) is an electronic parameter for a molecule, which used to discuss about the intermolecular interactions involving dipole forces. The increase in dipole moment cause an enhancement in the interaction between the inhibitor molecules and metal surface leading to stronger adsorption of inhibitor molecules on the surface and higher inhibition efficiency [20, 51]. The calculated dipole moment values for S₁ and S₂ show that S₂ with larger dipole moment can be adsorbed on the steel surface more easily than S₁. As a result, S₂ would be a better corrosion inhibitor as it was found in experimental data. In keeping with above expressions, we can deduced that the higher value of E_{HOMO} and lower value of ΔE as well as the possibility of $d\pi-d\pi$ bond formation due to presence of sulphur atom in S₂ molecule compensate the inappropriate value of E_{LUMO} compared with that of S₁.

4. CONCLUSION

It was found that the inhibition efficiencies of the Schiff bases S₁ and S₂ enhanced with increasing their concentration in the corrosive solution. Moreover, the obtained results with Tafel polarization method indicated that with addition of S₁ and S₂, I_{corr} decreased up to 31.4 and 14.1 $\mu\text{A cm}^{-2}$, respectively. The maximum displacement for E_{corr} was 53 mV toward anodic potentials showing that the Schiff bases acted as mixed type or adsorptive corrosion inhibitors with

predominantly anodic inhibition effect. The impedance measurements exhibited that the inhibitors adsorption on the carbon steel surface causes the polarization resistance to increase up to 850.1 and 1950.3 $\Omega \text{ cm}^2$ for S_1 and S_2 , respectively. The maximum inhibition efficiency was obtained 97 % for $1.0 \times 10^{-3} \text{ M}$ of S_2 . FFTCCV measurements showed that the rate of adsorption for S_1 is larger than the rate for S_2 , but the surface coverage and strength of adsorption bond for S_2 is larger than S_1 . DFT method at B3LYP/6-31G(d,p) level of theory was used to describe the effect of molecular structure and electronic properties on the inhibition efficiencies of studied Schiff bases. The higher value of inhibition efficiency for S_2 could be related to higher value of E_{HOMO} , lower value of ΔE as well as the presence of sulphur atom in its structure, which can form $d\pi-d\pi$ bond with 3d-electrons of Fe.

ACKNOWLEDGEMENTS

The authors express their appreciation to the University of Tehran Research Council for financial support of this work.

References

1. I. Ahamad, R. Prasad and M.A. Quraishi, *Corros. Sci.*, 52 (2010) 933
2. M. Abdallah and M.M. El-Naggar, *Mater. Chem. Phys.*, 71 (2001) 291
3. S. Issaadi, T. Douadi, A. Zouaoui, S. Chafaab, M.A. Khan and G. Bouet, *Corros. Sci.*, 53 (2011) 1484
4. R. Solmaz, *Corros. Sci.*, 52 (2010) 3321
5. P.A. Schweitzer, *Fundamentals of metallic corrosion: atmospheric and media corrosion of metals*, CRC Press, Taylor & Francis Group, second ed. (2007)
6. J.R. Davis, Davis & Associates, *Corrosion: understanding the basics*, ASM International, First printing (2000)
7. I. Ahamad, C. Gupta, R. Prasad and M.A. Quraishi, *J. Appl. Electrochem.*, 40 (2010) 2171
8. N.A. Negm, F.M. Ghuiba and S.M. Tawfik, *Corros. Sci.*, 53 (2011) 3566
9. M. Behpour, S.M. Ghoreishi, N. Mohammadi and M. Salavati-Niasari, *Corros. Sci.*, 53 (2011) 3380
10. M.A. Migahed, A.A. Farag, S.M. Elsaed, R. Kamal, M. Mostfa and H. Abd El-Bary, *Mater. Chem. Phys.*, 125 (2011) 125
11. M. Behpour, S.M. Ghoreishi, M. Salavati-Niasari and B. Ebrahmicu, *Mater. Chem. Phys.*, 107 (2008) 153
12. H. Ma, S. Chen, L. Niu, S. Zhao, S. Li and D. Li, *J. Appl. Electrochem.*, 32 (2002) 65
13. S. Chen and T. Kar, *Int. J. Electrochem. Sci.*, 7 (2012) 6265
14. S.S. Afak, B. Duran, A. Yurt and G. Turkoğlu, *Corros. Sci.*, 54 (2012) 251
15. A. Toropov, K. Nesmerak, I. Raska, K. Waisser and K. Palat, *Comput. Biol. Chem.*, 30 (2006) 434
16. Y.P. Zhou, C.B. Cai, S. Huan, J.H. Jiang, H.L. Wu, G.L. Shen and R.Q. Yu, *Anal. Chim. Acta*, 593 (2007) 68
17. T. Puzyn, A. Mostrag, N. Suzuki and J. Falandysz, *Atmos. Environ.*, 42 (2008) 6627
18. L. Carlsen, B.N. Kenessov and S.Y. Batyrbekova, *Environ. Toxicol. Pharmacol.*, 27 (2009) 415
19. A.R. Katritzky, D.C. Fara, R.O. Petrukhin, D.B. Tatham, U. Maran, A. Lomaka and M. Karelson, *Curr. Top. Med. Chem.*, 2 (2002) 1333
20. N.O. Obi-Egbedi and I.B. Obot, *Arabian J. Chem.*, 6 (2013) 211
21. I. Danaee, O. Ghasemi, G.R. Rashed, M. Rashvanavei and M.H. Maddahy, *J. Mol. Struct.*, 1035 (2013) 247

22. A.K. Singh, S. Khan, A. Singh, S.M. Quraishi, M.A. Quraishi and E.E. Ebenso, *Res. Chem. Intermed.*, 39 (2013)1191
23. A. Zarrouk, I. El Ouali, M. Bouachrine, B. Hammouti, Y. Ramli, E. M. Essassi, I. Warad, A. Aouniti and R. Salghi, *Res. Chem. Intermed.*, 39 (2013) 1125
24. S. John, K.M. Ali and A. Joseph, *Bull. Mater. Sci.*, 34 (2011) 1245
25. A. Yurt, S. Ulutas and H. Dal, *Appl. Surf. Sci.*, 253 (2006) 919
26. Y. Chen, Z. Tang, R. Tong and Q.Wang, *JCSCP.*, 27 (2007) 156
27. A. Guendouz, N. Missoum, A. Chetouani, S.S. Al-Deyab, B.B.Cheikhe, N. Boussalah, B. Hammouti, M. Taleb and A. Aouniti, *Int. J. Electrochem. Sci.*, 8 (2013) 4305
28. F. Faridbod, M.R. Ganjali, R. Dinarvand, P. Norouzi and S. Riahi, *Sensors*, 8 (2008) 1645
29. M.R. Ganjali, M. Tavakoli, F. Faridbod, S. Riahi, P. Norouzi and M. Salavati-Niassari, *Int. J. Electrochem. Sci.*, 3 (2008) 1559
30. F. Faridbod, M.R. Ganjali, R. Dinarvand, and P. Norouzi, *Comb. Chem. High Throughput Screening*, 10 (2007) 527
31. ASTM G3-89, *standard practice for conventions applicable to electrochemical measurements in corrosion testing* (1994)
32. K.C. Emregül, R. Kurtaran and O. Atakol, *Corros. Sci.*, 45 (2003) 2803
33. M.J. Frisch, G.W. Trucks, H.B. Schlegel, G.E. Scuseria, M.A. Robb, et al., Gaussian Inc., Wallingford CT (2004)
34. J.O.L. Riggs, *Corrosion Inhibitors*, second ed., (Ed.: C.C. Nathan), Houston, TX (1973)
35. E.S. Ferreira, C. Giancomelli, F.C. Giacomelli and A. Spinelli, *Mater. Chem. Phys.*, 83 (2004) 129
36. M.G. Hosseini, M. Ehteshamzadeh and T. Shahrabi, *Electrochim. Acta*, 52 (2007) 3680
37. N. Soltani, M. Behpour, S.M. Ghoreishi and H. Naeimi, *Corros. Sci.*, 52 (2010) 1351
38. C.S. Hsu and F. Mansfeld, *Corrosion*, 57 (2001) 747
39. M.R. Ganjali, P. Norouzi, R. Dinarvand, R. Farrokhi and A.A. Moosavi-Movahedi, *Mater. Sci. Eng. C*, 28 (2008) 1311
40. P. Norouzi, M.R. Ganjali and L. Hajiaghababaei, *Anal. Lett.*, 39 (2006) 1941
41. P. Norouzi, B. Larijani and M.R. Ganjali, *Int. J. Electrochem. Sci.*, 7 (2012) 7313
42. P. Norouzi, B. Larijani, M.R. Ganjali and F. Faridbod, *Int. J. Electrochem. Sci.*, 7 (2012) 10414
43. P. Norouzi, M.R. Ganjali, T. Alizadeh, and P. Daneshgar, *Electroanalysis*, 18 (2010) 947
44. P. Norouzi, V.K. Gupta, F. Faridbod, M. Pirali-Hamedani, B. Larijani and M.R. Ganjali, *Anal. Chem.*, 83 (2011) 1564
45. R. Dennington, T. Keith, J. Millam, *GaussView, Version 5*, Semichem: Shawnee Mission, KS (2009)
46. A.Y. Musa, W. Ahmoda, A.A. Al-Amiery, A.A.H. Kadhum and A.B. Mohamad, *J. Struct. Chem.*, 54 (2013) 301
47. N. Soltani, N. Tavakkoli, M. Khayatkashani, M.R. Jalali and A. Mosavizade, *Corros. Sci.*, 62 (2012) 122
48. Z. El Adnani, M. Mcharfi, M. Sfaira, M. Benzakour, A.T. Benjelloun and M. EbnTouhami, *Corros. Sci.*, 68 (2013) 223
49. M.S. Morad and A.M. Kamal El-Dean, *Corros. Sci.*, 48 (2006) 3398
50. H.D. Leçe, K.C. Emregül and O. Atakol, *Corros. Sci.* 50 (2008) 1460
51. P. Udhayakala, A. Jayanthi, T.V. Rajendiran and S. Gunasekaran, *Res. Chem. Intermed.* 39 (2013) 895